ARTICLES

Dynamics, Site Binding, and Distribution of Counterions in Polyelectrolyte Solutions Studied by Electron Paramagnetic Resonance Spectroscopy†

Dariush Hinderberger, Hans Wolfgang Spiess, and Gunnar Jeschke*

Max-Planck-Institut für Polymerforschung, Postfach 3148, 55021 Mainz, Germany

Received: July 15, 2003

A microscopic picture of counterion condensation in liquid and glassy frozen solutions of the cationic polyelectrolyte poly(diallyldimethylammonium chloride) (PDADMAC) is derived from data obtained by a combination of continuous-wave and pulse electron paramagnetic resonance techniques. The condensation of such divalent anions to the polyelectrolyte chain in the presence of a large excess of polyelectrolyte and monovalent counterions can be described by a dynamic equilibrium between specifically site-bound and nonspecifically territorially bound counterions with exchange between the two states proceeding on time scales significantly shorter than 1 ns. No free divalent counterions are detected. The dynamic electrostatic attachment is manifest in an axially symmetric rotational diffusion tensor, with the unique axis of fast rotation corresponding to the electrostatic bond between one sulfonate group of Fremy's salt and the quaternary ammonium group of the PDADMAC repeat unit. A distance of 0.43 nm between the electron spin and the ^{14}N nucleus of the ammonium group is found by electron spin−echo envelope modulation spectroscopy, suggesting that the site-bound state corresponds to contact ion pairs. The same experiment provides an estimate of 20% site-bound and 80% territorially bound divalent counterions in glycerol/water glassy frozen solution. Pulse electron−electron double resonance measurements show that on nanometer length scales the counterions are virtually homogeneously distributed in three dimensions for high polyelectrolyte concentration but linearly distributed along stretched chains at low polyelectrolyte concentrations where no overlap of chains is expected.

1. Introduction

Polyelectrolytes are macromolecular substances that are soluble in water or other ionizing solvents and dissociate into macromolecular ions that carry multiple charges (polyions) together with an equivalent amount of ions of small charge and opposite sign. They play an important role in fields of scientific research as diverse as molecular biology and nanotechnology.[1−4] Many biological macromolecules such as DNA or proteins are polyelectrolytes and use electrostatic interactions to trigger and control structural changes or binding of small molecules.[4] Synthetic polyelectrolytes are also applied commercially in cosmetics, fuel cells, and the food and oil industry.[5,6]

Highly charged biological as well as synthetic polymeric materials have already been under investigation experimentally and theoretically for several decades and it is commonly acknowledged that their interesting structural properties stem from the delicate balance of two opposing interactions. First, electrostatic repulsion between the like charges on each unit of the polyelectrolyte leads to a preference for extended conformations of the polyelectrolyte chain. Second, polyelectrolytes are usually dissolved in water or other solvents with high dielectric permittivity, which are poor solvents with respect to the polymer backbone (hydrocarbons). Poor solubility is equivalent to an attractive hydrophobic interaction between repeat units on the polyelectrolyte, which favors more collapsed structures.[1,7,8]

Despite numerous studies on polyelectrolytes, the combined effects of polyelectrolyte−counterion and polyelectrolyte−solvent interactions on polyelectrolyte structure are not fully understood. It is known that the screening of intramolecular electrostatic repulsion by oppositely charged counterions can lead to a dominance of hydrophobic attraction and thus to more collapsed, globular chain conformations.[9−11]

Characterization methods that probe macroscopic properties (such as conductivity) or can characterize long-range order (light, X-ray, and neutron scattering) have been applied extensively in the past.[1,2] Magnetic resonance methods, such as electron paramagnetic resonance (EPR) spectroscopy[12,13] on spin-carrying counterions, being local, sufficiently sensitive, and highly selective, should be able to provide complementary information on local, i.e., microscopic, structure and dynamics of polyelectrolyte materials. Ionic spin probes, which substitute for low molecular weight counterions, have been used previously to gain detailed information on structure and dynamics of polymer systems containing charges.[14−19]

Using continuous-wave (CW) and Fourier transform (FT) EPR spectroscopy of divalent and trivalent spin probes in mixtures of water and organic solvents (ethanol, *N*-methylpropionamide) at room temperature, we could demonstrate that counterions are condensed to cationic polyelectrolyte chains via *dynamic electrostatic attachment*, which can be pictured as

† Dedicated to Jack H. Freed on the occasion of his 65th birthday.

* Corresponding author. Tel.: +49-6131-379 126. Fax: +49-6131-379 100. E-mail: jeschke@mpip-mainz.mpg.de.

10.1021/jp036043u CCC: $27.50
Published on Web 02/24/2004

CHART 1: Molecular Structures of Charged Spin Probe, Polyelectrolyte, and Solvents Used in This Study[a]

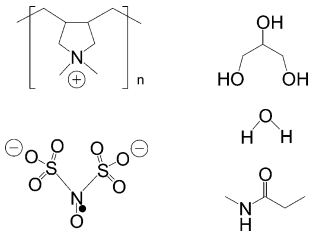

[a] Key: FS, Fremy's salt dianion; PDADMAC, poly(diallyldimethylammonium chloride); NMPA, *N*-methylpropionamide

formation and breaking of contact ion pairs on the subnanosecond time scale.[14] Moreover, we found that the effect of solvent in these systems is more complex than just that of a dielectric continuum between charges. Changing relative permittivity from $\epsilon \approx 50$ (ethanol/water 1:1) to $\epsilon \approx 140$ (*N*-methylpropionamide (NMPA)/water 2.3:1) did not result in dramatic changes of the time scale of dynamic electrostatic attachment and of local concentrations of probe ions, whereas the results for both these solvents differed strongly from the results for pure water with intermediate relative permittivity ($\epsilon \approx 80$). We attributed this to the interaction of the hydrophobic parts of organic solvent molecules with the polymer backbone, which leads to a screening of hydrophobic interactions and thus prevents conformational changes that occur in pure water.

The same holds true in the more viscous solvent mixture glycerol/water (wt 2:1, $\epsilon \approx 58$).[19] In this case, we could furthermore indirectly observe a slowing down of the polyelectrolyte chain dynamics by measuring the rate of rotational diffusion of the dynamically attached counterions that depends on polyelectrolyte concentration.

In this work we analyze rotational diffusion of contact ion pairs formed by charged spin probes and polyelectrolyte repeat units in more detail and use more sophisticated pulse EPR experiments to obtain structural information on the polyelectrolyte−counterion system in frozen glassy solution. Our study is organized as follows. In the first part we fit experimental spectra of a dianionic nitroxide spin probe in a fluid solution of oppositely charged polyelectrolyte in NMPA or ethanol/water by a simple model of anisotropic rotational diffusion[20] combined with exchange broadening caused by high local concentration of counterions in the vicinity of the polyelectrolyte. This analysis aims to quantify the effect of dynamic electrostatic attachment on rotational diffusion of the spin-carrying counterions. In the second part, we apply three-pulse electron spin−echo envelope modulation (ESEEM) in frozen glassy solution to obtain information on the geometric structure and fraction of putative contact ion pairs. Finally, we present data from four-pulse double electron−electron resonance (DEER) measurements[21] that are related to the pair correlation function of the spin-carrying counterions on a nanometer length scale[22,23] and model these data by assuming contributions due to spin-carrying counterions that are homogeneously distributed in three dimensions or one-dimensionally distributed along isolated locally stretched polyelectrolyte chains.

2. Materials and Methods

As spin probe (Chart 1) we used Fremy's salt dianion (potassium nitrosodisulfonate), FS, technical grade (ICN Biomedicals). As cationic polyelectrolyte we chose poly(diallyldimethylammonium chloride), PDADMAC, with an M_w of 240 000, (Polysciences, Inc.). Both chemicals were used as received.

As solvent systems we chose deionized Milli-Q-water (permittivity: $\epsilon_r = 80$ at 293 K), 66 wt % glycerol/34 wt % water (made from 87 wt % glycerol/water mixture, Fluka, density $\rho \approx 1.17$ g/mL, approximate $\epsilon_r = 57$ at 293 K) and 70 vol % *N*-methylpropionamide (Aldrich Chemical Co.)/30 vol % water (NMPA/H_2O, $\rho = 0.95$, approximate $\epsilon_r = 140$ at 293 K). Small amounts of KOH were added to adjust the solutions to pH > 8. Spin probe (FS) concentration was fixed at 0.5 mM, and polyelectrolyte concentration was varied from 4 mM (in repeat units) to 140 mM. Data are presented as a function of the ratio *R* of spin probes to polymer repeat units, so that no assumption on the actual number of repeat units per chain, and thus on M_n, had to be made.

EPR spectra in solution at X-band (9.7 GHz) were measured on a Bruker ELEXSYS 580 spectrometer using an AquaX inlet and a rectangular cavity (4103TM, Q-values typically 3000). The temperature during these measurements was 293 K.

Pulse EPR experiments were performed on the same spectrometer using a dielectric resonator (MD4EN). The temperature was set to 80 K by cooling with liquid nitrogen using an Oxford cryostat and cooling system. Glycerol/water (2:1) was used as a solvent for pulse EPR experiments at low temperatures as only samples in this solvent mixture were found to reliably form frozen glassy solutions. The samples were shock-frozen by immersion of the sample tubes into liquid nitrogen before loading them into the cooled cavity.

CW EPR. CW EPR spectra of FS in different solutions of PDADMAC were fitted in the following manner. The spectral simulation program by Schneider and Freed[20] was used to provide initial approximate fits for the relative intensities of the three lines of the nitroxide spectrum assuming an intrinsic line width, as observed in the absence of polyelectrolyte and thus neglecting Heisenberg exchange or dipolar broadening due to enhanced local concentration. This rough preliminary fit (absorption spectrum) was then Fourier transformed to give the time-domain data $V_{sim}(t)$, and a convolution with an empirical broadening function (stretched exponential function) was performed to account for concentration broadening:

$$V(t) = V_{Sim}(t)\,\exp(-(kt)^x) \qquad (1)$$

where *k* is a characteristic decay time constant related to average concentration and *x* is the stretch factor characterizing the width of the distribution of concentrations. After inverse Fourier transformation and pseudomodulation[24] a derivative-mode spectrum was obtained. This convolution affects the narrower low-field and center-field lines more strongly than the high-field line that is already significantly broadened by slowed rotational diffusion. The stretched exponential broadening function accounts for the distribution of local concentrations of the FS counterions, i.e., for the decrease of local concentration with increasing distance from the polyelectrolyte chain. This empirical broadening function is used as an approximation of a physically motivated broadening function that could be derived from a model for the radial distribution function of counterions[25,26] and a calibration of the concentration dependence of the line width. The full analysis of all our data sets using such a physically motivated broadening function is beyond the scope of the present work and will be published later. Preliminary checks have shown that the stretched exponential function in eq 1 reproduces line shapes obtained with more sophisticated broadening functions within experimental precision, so that the information of dynamics derived from the present analysis is reliable.

Pulse EPR. To characterize electron−nuclear hyperfine couplings, we use the stimulated echo sequence $(\pi/2)-\tau-(\pi/2)-T-(\pi/2)-\tau-$echo with the usual four-step phase cycling[27] to eliminate unwanted echoes. The evolution time increment ΔT is 16 ns. Hyperfine coupling of the electron spin to remote nuclei of a certain isotope causes modulation of the stimulated echo with the nuclear Zeeman frequency of that isotope. The depth of the modulation and its decay contain information on the electron-spin-to-nucleus pair correlation function. This information is conveniently extracted by ratio analysis,[28] in which the ratio of the upper envelope (connecting the maxima of the modulation) to the lower envelope (connecting the minima of the modulation) is computed and then fit to a simulated ratio. The simulation assumes that due to the r^{-6} dependence of the modulation depth on electron−nuclear distance r the modulation is dominated by the shell of nuclei of the given isotope that is closest to the paramagnetic center. Modulation depth and decay depend on the radius r_1 of this shell, the isotropic hyperfine coupling a, and the average number n of nuclei in the closest shell. Although such a model strongly simplifies the situation in a disordered system, it can provide useful estimates for the distance of closest approach between a paramagnetic and a diamagnetic molecule. Ratio analysis was performed with a homewritten program in MATLAB (The MathWorks, Inc.), which is available on request from the authors.

Four-pulse DEER experiments were performed with the sequence $(\pi/2)_{\nu A}-\tau_1-(\pi)_{\nu A}-t'-(\pi)_{\nu B}-(\tau_1+\tau_2-t')-(\pi)_{\nu A}-\tau_2-$echo, $(+x, -x)$ phase cycling of the first pulse, and averaging over 25 increments of τ_1 ($\Delta\tau_1 = 8$ ns) to suppress proton modulations.[21,23] Here, ν_A is the observer frequency (local maximum at the low-field edge of the EPR absorption spectrum) and ν_B the pump frequency (global maximum of the EPR absorption spectrum, $\nu_B = \nu_A - 56$ MHz). The time t' after the first π-pulse is incremented, and the pulse lengths and delays are as follows: $(\pi/2)_{\nu A} = 16$ ns, $(\pi)_{\nu A} = 32$ ns, $(\pi)_{\nu B} = 12$ ns, $\tau_1 = 200$ ns, $\tau_2 = 2\mu$s, $\Delta t' = 8$ ns, $t'_0 = 80$ ns. DEER time traces were fitted by varying a concentration c_{hom} corresponding to a fraction of spin probes homogeneously distributed in three dimensions and a linear density c_{lin} corresponding to an equal distribution in one dimension in the pair correlation function:

$$G(r) = c_{hom}N_A + c_{lin}/r^2 \qquad (2)$$

where N_A is Avogadro's constant, c_{hom} is in units of mmol/L (mol/m^3), and c_{lin} in units of m^{-1}. The time traces were computed from the pair correlation function using the shell factorization model described previously.[22] This approach to data analysis is analogous to an approach used earlier by Milov and Tsvetkov in work on chain conformation of spin-labeled poly(vinylpyridine).[29]

3. Results

3.1. Analysis of CW EPR Spectra in Liquid Solution. A typical CW EPR spectrum of FS/PDADMAC ($R = 0.011$) in NMPA/water is shown in Figure 1 together with a superimposed simulation (dotted line). Note that the lines deviate strongly from a Lorentzian shape, as is manifest in the stretch factor $x = 0.1$ of the empirical broadening function ($k = 1.8 \times 10^{13}$ s^{-1}). Indeed, we found it impossible to fit the spectra assuming a single well-defined value for the Heisenberg exchange frequency in the simulation program.[20] Rotational diffusion can be described by an axial tensor with the unique axis along the N−S bond of FS, as indicated in Figure 2. Rotation about this preferred axis is approximately 80-fold faster than about axes perpendicular to it ($d_{||} = 3.7 \times 10^9$ s^{-1}, $d_\perp = 5.5 \times 10^7$ s^{-1}). These diffusion rates are approximately 1 ($d_{||}$) and 3 ($d_\perp$) orders of magnitude slower than for the almost isotropic rotational diffusion of FS in the same solvent mixture in the absence of polyelectrolyte (data not shown). The relative intensities of the three lines in the experimental spectrum clearly exclude an axially symmetric rotational diffusion tensor with the unique axis along the bisector of the two N−S bonds, i.e., along the C_2 symmetry axis of the radical (see inset in Figure 1).

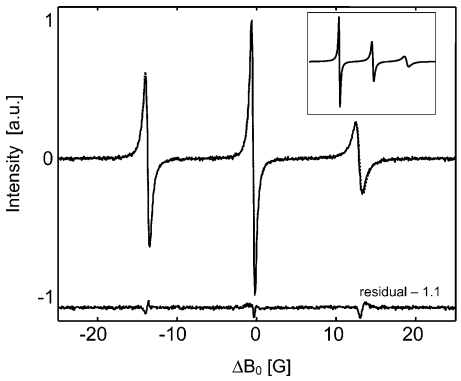

Figure 1. X-band (9.77 GHz) EPR spectrum (solid line) of FS + PDADMAC ($R = 0.011$, 46 mM PDADMAC) in 70% NMPA/30% water at 293 K. A simulation as described by eq 1 in the text, assuming preferred rotation about the axis indicated in Figure 2, is superimposed (dotted line) and the residual of the experimental and the simulated spectrum is shown. The inset shows a simulation of a spectrum assuming preferred rotation about the C_2 symmetry axis of the FS molecule.

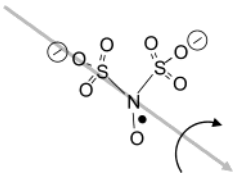

Figure 2. Sketch of the rotational diffusion tensor underlying the simulation of experimental CW EPR spectra (e.g., that in Figure 1). The gray arrow marks the direction parallel to the axis of fast rotation; the axes of slow rotation are perpendicular to this axis. The rotational rates corresponding to the two principal rotations are $d_{||} = 3.7 \times 10^9$ s^{-1}, and $d_\perp = 5.5 \times 10^7$ s^{-1}.

By application of this combination of slow tumbling line shape simulation and convolution with an empirical broadening function described in section 2, experimental spectra can be nicely fit throughout the whole range of polyelectrolyte concentration ($0.0036 \le R \le 0.125$). Although parameters k and x in eq 1 vary strongly (data not shown), which indicates substantial changes in the radial distribution of concentrations, the rotational diffusion tensor is found to be almost independent of polyelectrolyte concentration. Over the whole range of concentrations studied here, the rotational diffusion rates decrease only by approximately 10% with increasing polyelectrolyte concentration. The stretch factor x increases with decreasing polyelectrolyte concentration, indicating a more heterogeneous counterion distribution in dilute solution. This is in agreement with our previous findings[14] and with theoretical expectations.[25,26]

3.2. Pulse EPR Experiments in Frozen Solution. *Three-Pulse ESEEM.* Typical three-pulse ESEEM data for FS in the presence of PDADMAC ($R = 0.011$) are shown in Figure 3. After division of the time-domain signal by the stimulated echo decay (approximated by a stretched exponential function), maxima and minima of the modulation curve are extracted by polynomial fitting of the experimental trace, and upper and lower

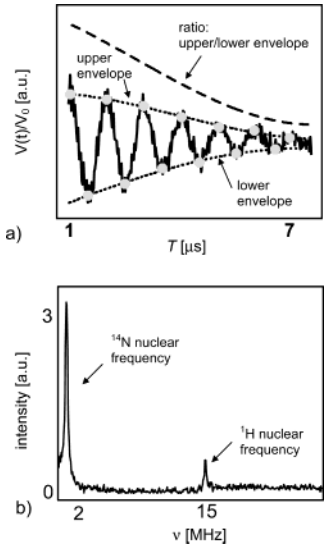

Figure 3. Time-domain and frequency-domain data from three-pulse ESEEM (X-band, 9.77 GHz) measurement of FS + PDADMAC (R = 0.011, 46 mM PDADMAC) in glycerol/water. (a) Time-domain data after division by a stretched exponential decay (solid line): filled gray circles, maxima and minima of ^{14}N modulation; dotted lines, upper and lower envelopes of ^{14}N modulation; dashed line, ratio of upper/lower envelope. (b) Frequency-domain data (Fourier transform of time-domain data) with the peaks at the nuclear Zeeman frequencies of ^{14}N (∼1.1 MHz) and ^{1}H (∼14.7 MHz) marked;

envelopes are then determined by polynomial fitting of the maxima and minima, respectively (Figure 3a). In the Fourier transform of the time-domain signal (Figure 3b) sharp and narrow peaks were observed at a frequency of 1.1 MHz, which is the nuclear Zeeman frequency of a ^{14}N nuclear spin at the static field $B_0 \gg 346$ mT used in our experiments. In the absence of polyelectrolyte, no modulation was observed at this frequency. We therefore assign the measured modulation to the quaternary nitrogen in the PDADMAC repeat unit (Chart 1). The unusually narrow ^{14}N ESEEM line is due to the nearly tetrahedral symmetry of the quaternary nitrogen, which leads to a small nuclear quadrupole coupling. Indeed, DFT (ADF 2002.01 package,[30] BLYP density functional, TZ2P basis set) calculations of quadrupole couplings of quaternary ^{14}N nuclei provide values of approximately $e^2qQ/h = 200$ kHz. Note that all data were recorded with $\tau = 200$ ns, corresponding to a blind spot for the modulation due to ^{1}H nuclei,[27] so that modulation due to ^{14}N nuclei dominates, which significantly simplifies data analysis.

No general trend for the fit parameters r_1, a, and n was found when polyelectrolyte concentration was varied. We find an electron−nuclear distance of closest approach of $r_1 \approx 0.43$ nm, a virtually negligible isotropic hyperfine coupling of $a \approx 0.07$ MHz, and an average number of $n \approx 0.20$ ^{14}N nuclei in the shell of closest approach. Although this kind of data analysis is strictly valid only for spherical coordination shells and neglect of angular correlation,[27,28] we may assume that it is a good approximation in the present case where the number of nuclei at closest approach for a given electron spin is usually 0 or 1. Neglect of nuclear quadrupole coupling probably introduces an error mainly in a but may also lead to a slight underestimate in r_1. For comparison, we performed force-field (MMFF94 force field in SPARTAN, Wavefunction, Inc.) calculations of two FS molecules and a short section of a PDADMAC chain with twelve monomeric units to get an estimate of an electrostatic closest approach. It is found that in such a model system in a vacuum the closest distance between the nitrogen atom of the

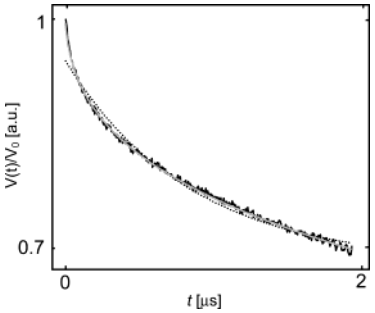

Figure 4. Four-pulse DEER time trace (EPR frequency 9.3 GHz) of FS + PDADMAC (R = 0.022) in glycerol/water with two different fits; solid black line, experimental time trace; dotted black line, best fit with single-exponential decay; solid gray line, best fit corresponding to the pair correlation function described by eq 2.

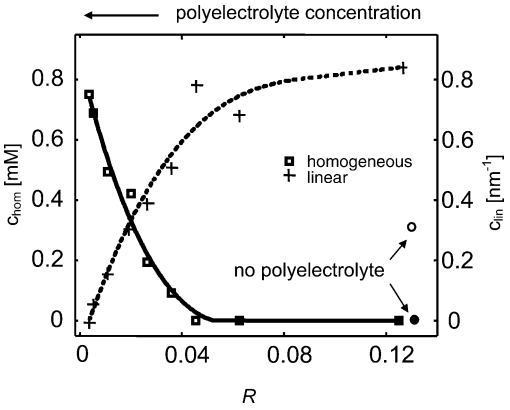

Figure 5. Extracted contributions of three-dimensional (homogeneous) and one-dimensional (linear) distributions of FS from fitting the parameters c_{hom} and c_{lin} of eq 2 to four-pulse DEER time traces (EPR frequency 9.3 GHz) of FS + PDADMAC in the whole R range investigated in glycerol/water: open squares, homogeneous concentration c_{hom}; crosses, linear concentration c_{lin}; open circle, c_{hom} of FS in glycerol/water without PDADMAC; filled circle, c_{lin} of FS in glycerol/water without PDADMAC. Solid and dotted black lines are meant as guides to the eye.

FS nitroxide group and the charge-bearing ammonium ion on the PDADMAC chain is approximately 0.4 nm, and thus rather close to the values found from ratio analysis of ESEEM data.

Four-Pulse DEER. Typical experimental four-pulse DEER data of FS in solutions of PDADMAC (R = 0.022) are displayed in Figure 4 together with the best fit by a single exponential decay (dotted line) and by the two-state model corresponding to the pair correlation function described by eq 2 (solid gray line). The fit by a single exponential function significantly deviates from experimental data, whereas the model with one fraction of spin-carrying counterions that is homogeneously distributed in three dimensions and another fraction that is equally distributed along only one dimension fits the data within experimental precision. The former fraction dominates the long time behavior, whereas the latter one is responsible for the fast decay at short times. Plots of the two fit parameters c_{hom} and c_{lin} for experimental data in the whole range of R values (Figure 5) show that at high polyelectrolyte concentration (low R values), DEER time-domain data are dominated by three-dimensionally distributed spins, which have a significantly higher concentration c_{hom} than the used bulk concentration of 0.5 mM. At intermediate concentrations ($0 < R < 0.05$) both a three-dimensionally and a one-dimensionally distributed fraction of probe ions are present in the system. The former fraction decreases and the latter fraction increases upon reduction of polyelectrolyte concentration (increase of R). At $R > 0.05$, the

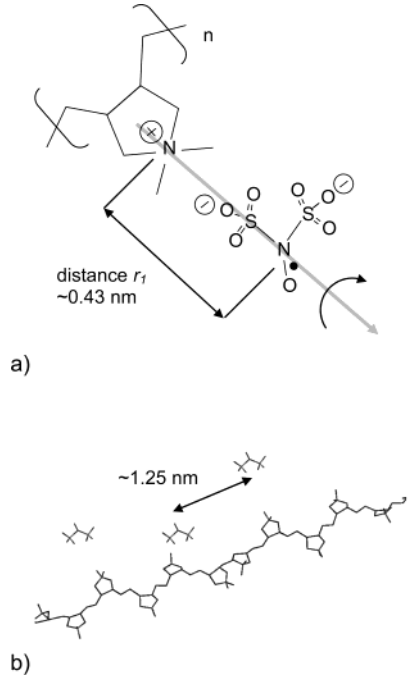

Figure 6. Sketches of geometry and dynamics of FS counterions condensed to a PDADMAC chain. (a) Sketch of the local geometry of an FS spin probe that is site-bound to a PDADMAC ammonium group. The gray arrow depicts the direction parallel to the axis of fast rotation of FS (see Figure 2). The distance $r_1 \gg 0.43$ nm was obtained from ratio analysis of three-pulse ESEEM data (see Figure 3). (b) Sketch of the assumed linear distribution of FS spin probes along a rather elongated PDADMAC chain. The estimate for the average distance of 1.25 nm was found from the maximum of linear spin density $c_{lin} \approx 0.8$ nm^{-1} (Figure 5).

three-dimensionally distributed fraction is insignificant, and the DEER time traces can be fit by an equal distribution of spins along a linear object. The value for linear spin probe density c_{lin} attains a plateau value of ~ 0.8 nm^{-1} for $R > 0.05$.

4. Discussion

Anisotropic Dynamics of FS Spin Probe in a Liquid Solution of PDADMAC. As discussed previously, CW EPR spectra of FS in liquid solutions of PDADMAC are governed by two features: rotational diffusion of FS spin probe and the heterogeneity of local concentration of FS.[14,19] The convolution approach introduced here now allows for a better discrimination of these two effects. Figure 6a depicts how the local geometry of the short-lived contact-ion pair of FS and PDADMAC is reflected in the rotational diffusion tensor. During the time of the site binding, rotation around the electrostatic bond formed between ammonium and the sulfonate group can still be fast, as the potential of the electrostatic bond is not significantly altered during the rotation and sterical hindrance may be weak. However, rotation perpendicular to this direction is slowed strongly, as it is coupled to the collective motion of the polyelectrolyte chain. This slowing down of rotation about the axes perpendicular to the electrostatic bond during site binding probably corresponds to a factor much larger than 80, as the PDADMAC chains are long (on average $\sim$1500 monomeric units) and the polyelectrolyte rotational motion is slower than that of freely rotating FS by orders of magnitude. Because of rapid exchange of FS spin probes between the attached (site-bound) and detached (territorially bound) state, the rotational diffusion tensor is a time average over the almost isotropic reorientation of detached spin probes and the uniaxial reorientation of attached spin probes. The weak dependence of the rotational diffusion tensor on polyelectrolyte concentration indicates that the rate of this exchange between attached and detached states does not depend on R for $R \ll 1$, i.e., for a large excess of poylelectrolyte repeat units with respect to the spin-carrying divalent counterions.

In fact, such analysis of the complex rotational dynamics imposed by dynamic electrostatic attachment in terms of Brownian diffusion with an axially symmetric rotational diffusion tensor amounts to a considerable simplification that comes at the expense of loosing some information on microscopic details of the process. It would be intriguing to characterize such details by resorting to more sophisticated models of rotational diffusion such as the model of slowly relaxing local structure introduced by Polimeno and Freed.[31] However, for our present data sets such an approach does not seem to be warranted, as the fits with the more simple model of Brownian diffusion are virtually perfect. Concurrent analysis of data obtained at X-band (9.4 GHz) and W-band (94 GHz) frequencies with water/glycerol mixtures as a solvent may provide the stronger constraints that are required for such a more detailed model and is planned for the future.

An intriguing consequence of the good fit of the present data by the described dynamical model is that on the time scales governing the EPR line shapes the site binding of the divalent FS spin probe mostly proceeds via only one of its sulfonate groups, not by forming a locally neutral aggregate with two repeat units. A model of fast hopping between two geometries of attachment involving both sulfonate groups can also be excluded, as it should lead to an effective preferred rotation axis along the C_2 symmetry axis of the radical dianion, which is clearly at variance with the relative line intensities in the experimental spectra (Figure 1). In earlier work we found some indication that in pure water as solvent, where hydrophobic attraction of monomeric units is not screened, small fractions of FS already suffice to induce a conformational change from more elongated to more globular structures, which might in turn suggest that FS ions connect two repeat units of the same chain (electrostatic cross-linking).[14] As spectra in water exhibit a very similar pattern of relative line intensities and can thus be explained by the same model of uniaxial rotational diffusion, this now appears to be unlikely. Rather the conformational change induced by divalent counterions may be due to compensation of a larger fraction of the polyelectrolyte charge compared to the case of monovalent counterions and may thus be caused by a change in the electrostatic potential rather than by electrostatic cross-links.

Relation of Glassy Frozen Solutions to Liquid Solutions. We have shown earlier that at room temperature the PDADMAC/FS system in glycerol/water mixtures behaves in a qualitatively similar manner as in NMPA/water as a solvent.[19] During shock-freezing of such a glass-forming system, we may assume that thermodynamic equilibrium can be reached at each temperature as long as typical rates for conformational changes, redistribution of counterions, etc. are faster than the cooling rate. With approach to the glass transition temperature, viscosity increases dramatically and the rates of all dynamic processes decrease by orders of magnitude. We therefore assume that the state of the system after shock-freezing is an ensemble of static structures (a "snapshot") roughly corresponding to the distribution of structures at the glass transition temperature of approximately 180 K. Although this is a significantly lower temperature than the one at which liquid solutions were studied

by CW EPR spectroscopy, we suppose that the same general phenomena occur and that the same general structural model for the polyelectrolyte−counterion system can be used in the discussion. Note, however, that *quantitative* findings for the glassy state cannot simply be assumed to pertain also to liquid solution.

FS−PDADMAC Distance in Frozen Solution: Characterization of Site Binding. With the results from ratio analysis of three-pulse ESEEM data we have direct evidence for electrostatic attachment (site binding) of FS to PDADMAC monomeric units. Together with the performed force field calculations, the estimate of approximately 0.43 nm for the electron−^{14}N distance is a clear indication that contact ion pairs are formed, i.e., that for some counterions no solvent molecules are located between the two oppositely charged moieties (ammonium and sulfonate groups). Figure 6a is a representation of the combination of this finding with the results for the rotational diffusion tensor of FS in PDADMAC. For all polyelectrolyte concentrations studied ($R \ll 1$), the coordination number of ^{14}N nuclei is approximately 0.2. Hence at a given time only 20% of FS spin probes form such contact ion pairs with PDADMAC chain monomer units, regardless of the ratio of spin probes to polyelectrolyte repeat units. Figure 6a thus only gives a *snapshot* of the attached state in what we call *dynamic electrostatic attachment*. Counterion attachment corresponds to the site-bound state in a dynamical equilibrium

$$(\text{free} \rightleftarrows) \text{ territorial binding} \rightleftarrows \text{site binding}$$

Dynamic information from CW EPR spectra in liquid solution indicates that the rate constant for the exchange between territorially bound and site-bound spin-carrying counterions is significantly larger than 10^9 s^{-1}. If the lifetime of the site-bound (attached) state were of the order of 1 ns or longer, we should observe bimodal spectra, i.e., a superposition of two dynamic components corresponding to territorially bound and site-bound FS probes. Furthermore, in the presence of polyelectrolyte there is no spectral component with line widths and relative intensities as observed in the absence of polyelectrolyte. This excludes the existence of a significant fraction of free divalent spin-carrying counterions. Such a picture, where at any given time all the FS counterions are either territorially bound or site-bound is also consistent with the fact that the exchange between these two states is very fast, which requires that diffusion lengths are short. The picture is also in agreement with simple polyelectrolyte theory, which predicts our systems to be in the regime of saturated counterion condensation of divalent FS spin probes.[13]

FS Distribution along the PDADMAC Chain. From the typical time-domain signal shown in Figure 4 it is obvious that the distribution of FS at least in solutions with medium and low PDADMAC content is certainly not homogeneous throughout the whole solution. The two-state model of a homogeneous three-dimensional distribution and an equal distribution along one dimension is the most simple model that leads to excellent fits of experimental data. The two curves of Figure 5 can be interpreted as the transition from a network of overlapping polyelectrolyte chains at high PDADMAC concentrations to a regime of isolated and extended polyelectrolyte chains at low concentration. In the former case, FS spin probes are distributed in the polymer network, which corresponds to only part of the volume of the whole solution, which explains that the c_{hom} values are larger than the bulk concentration. With decreasing concentration, the single chain character increases and c_{lin} becomes larger.

Note that the local concentration gradient (spatial distribution) of FS that leads to the distribution of line widths in CW EPR spectra (stretched exponential as a time-domain broadening function) corresponds to the *radial* direction with respect to the presumed elongated PDADMAC chains, whereas the linear density deduced from the DEER experiment corresponds to the direction along the PDADMAC chains. Under the conditions of our experiments, the DEER experiments are sensitive to distances up to approximately 5 nm.[22,23] Because for $R > 0.05$ the spin-carrying counterions are distributed linearly, it is safe to draw the conclusion that the PDADMAC chains have a minimum persistence length of approximately 5 nm.

The plateau value of 0.8 nm^{-1} for c_{lin} corresponds to an average distance between divalent spin-carrying counterions of approximately 1.25 nm (see Figure 6b). This seems to be the highest loading of the chain with these counterions that can be detected by the four pulse DEER measurements.

As only 20% of FS spin probes are site-bound, this finding includes the territorially bound spin probes. We may thus conclude that the distance of most of the territorially bound FS from the PDADMAC chains cannot be much larger than roughly 1 nm; otherwise the experimental data would not be perfectly fit by a linear distribution. This is in qualitative agreement with the theoretically predicted radial distribution function by Deshkovski et al.,[26] in which the counterion concentration for saturated counterion condensation decays as $c(r) \propto r^{-2}$. The finding is also again consistent with the requirement of short diffusion lengths imposed by observation of fast exchange between site-bound and territorially bound counterions.

5. Conclusion

For the first time, quantitative information was obtained on the structure, dynamics, and spatial distribution of contact ion pairs formed by site binding of divalent counterions to a polyelectrolyte. Simulations of CW EPR spectra of spin-carrying FS counterions in liquid solution in the presence of PDADMAC polyelectrolyte demonstrate that the lifetime of the electrostatically site-bound state is significantly less than 1 ns and that at such short time scales site binding preferentially proceeds via only one of the sulfonate moieties, whereas the other sulfonate group is interacting with PDADMAC charges through nonspecific electrostatic forces. The average rotational diffusion tensor for probe ions at dynamic equilibrium between the site-bound and territorially bound states is strongly anisotropic with approximately 80-fold faster rotation about an axis parallel to the formed electrostatic bond.

Pulse EPR techniques were applied to frozen glassy solutions of the FS/PDADMAC system to characterize the local structure of contact ion pairs and the distribution of the counterions along the chain. By ratio analysis of three-pulse ESEEM data, we obtained an estimate of 0.43 nm for the distance of closest approach between the electron spin of FS and the ^{14}N nucleus in the PDADMAC repeat unit, which agrees with the distance expected for a contact ion pair. Irrespective of polyelectrolyte concentration, the fraction of such site-bound FS spin probes is found to be close to 20%, with the remainder of the spin probes being bound territorially by nonspecific electrostatic interaction.

Local concentrations for a three-dimensional, homogeneous distribution of spin-carrying counterions and linear counterion densities were obtained for solutions with different polyelectrolyte concentrations by fitting four-pulse DEER data. At high polyelectrolyte concentrations, the FS spin probes are diluted into PDADMAC networks and thus distributed three-dimen-

sionally with larger concentrations than the bulk concentration, whereas at low PDADMAC concentration, FS ions exhibit a one-dimensional distribution due to attachment or territorial binding to single polyelectrolyte chains. An estimate of approximately 5 nm for the minimum persistence length of the PDADMAC chain and of 1.25 nm for the average FS−FS distance at maximum counterion loading could be obtained.

The radial distribution of local concentrations of FS ions was included in simulations of CW EPR spectra by convolution of the simulated spectra with an empirical broadening function. Quantitative analysis of this type of concentration broadening based on theoretical predictions about the radial distribution is now in progress.

Acknowledgment. We thank K. Kremer, C. Holm, P. Pincus, and A. R. Khokhlov for helpful discussions and C. Bauer for technical support.

Note Added in Proof. New simulations suggest that the plateau at $R > 0.05$ indicated by the dotted line in Figure 5 is caused by the inability of the DEER experiment to detect spin pairs with distances shorter than approximately 1.5 nm. Actual linear densities at R values larger than 0.05 may thus exceed the ones indicated by our measurements.

References and Notes

(1) Sukant, T., Jayant, K., Singh, N. H., Eds. *Handbook of Poylelectrolytes and Their Applications*; American Scientific Publishers: Stevenson Ranch, 2002.
(2) Dautzenberg, H.; Jaeger, W.; Kötz, J.; Philip, B.; Seidel, C.; Stscherbina, D. *Polyelectrolytes*; Hanser-Verlag: München, 1994.
(3) Decher, G. *Science* **1997**, *277*, 1232.
(4) Kumar, S.; Nussinov, R. *ChemBioChem* **2002**, *3*, 604.
(5) Ogawa, S.; Decker, E. A.; McClements, D. J. *J. Agric. Food Chem.* **2003**, *51*, 2806.
(6) Lee, S. H. *Polym. J.* **2000**, *32*, 716.
(7) Manning, G. S. *J. Chem. Phys.* **1969**, *51*, 924.
(8) Manning, G. S. *Acc. Chem. Res.* **1979**, *12*, 443.
(9) Kantor, Y.; Kardar, M. *Phys. Rev. E* **1995,** *51*, 1299.
(10) Dobrynin, A. V.; Rubinstein, M.; Obukhov, S. P. *Macromolecules* **1996,** *29*, 2974.
(11) Limbach, H. J.; Holm, C.; Kremer, K. *Europhys. Lett.* **2002**, *60*, 566.
(12) Freed, J. H. *Annu. Rev. Phys. Chem.* **2000**, *51*, 655.
(13) Atherton, N. M. *Principles of Electron Spin Resonance*; Ellis Horwood Limited: New York 1993.
(14) Hinderberger, D.; Jeschke, G.; Spiess, H. W. *Macromolecules* **2002,** *35*, 9698.
(15) Xue, H. Q.; Bhowmik, P.; Schlick, S. *Macromolecules* **1993**, *26*, 3340.
(16) Tsagaropoulos, G.; Kim, J. S.; Eisenberg, A. *Macromolecules* **1996**, *29*, 2222.
(17) Schädler, V.; Franck, A.; Wiesner, U.; Spiess, H. W. *Macromolecules* **1997**, *30*, 3832.
(18) Cramer, S. E.; Jeschke, G.; Spiess, H. W. *Macromol. Chem. Phys.* **2002**, *203*, 182.
(19) Hinderberger, D.; Spiess, H. W.; Jeschke, G. *Macromol. Symp.*, in press.
(20) Schneider, D. J.; Freed, J. H. In *Spin Labeling—Theory and Applications*; Berliner, L. J., Reuben, J., Eds.; Biological Magnetic Resonance, Vol. 8; Plenum Press: New York, 1989; Chapter 1.
(21) Pannier, M.; Veit, S.; Godt, A.; Jeschke, G.; Spiess, H. W. *J. Magn. Reson.* **2000**, *142*, 331.
(22) Jeschke, G.; Koch, A.; Jonas, U.; Godt, A. *J. Magn. Reson.* **2002**, *155*, 72.
(23) Jeschke, G. *ChemPhysChem* **2002**, *3*, 927.
(24) Hyde, J. S.; Pasenkiewicz-Gierula, M.; Jesmanowicz, A.; Antholine, W. E. *Appl. Magn. Reson.* **1990**, *1*, 483.
(25) Fuoss, R. M.; Katchalsky, A.; Lifson, S. *Proc. Natl. Acad. Sci. U.S.A.* **1951**, *37*, 579.
(26) Deshkovski, A.; Obukhov, S.; Rubinstein, M. *Phys. Rev. Lett.* **2001**, *86*, 2341.
(27) Schweiger, A.; Jeschke, G. *Principles of Pulse Electron Paramagnetic Resonance*; Oxford University Press: Oxford, U.K., 2001.
(28) Ichikawa, T.; Kevan, L.; Bowman, M. K.; Dikanov, S. A.; Tsvetkov, Yu. D. *J. Chem. Phys.* **1979**, *71*, 1167.
(29) Milov, A. D.; Tsvetkov, Yu. D. *Appl. Magn. Res.* **1997**, *12*, 495.
(30) te Velde, G.; Bickelhaupt, F. M.; Baerends, E. J.; Fonseca Guerra, C.; van Gisbergen, S. J. A.; Snijders, J. G.; Ziegler, T. *J. Comput. Chem.* **2001**, *22*, 93.
(31) Polimeno, A.; Freed, J. H. *J. Phys. Chem.* **1995**, *99*, 10995.